OPEN ACCESS

University of BRISTOL

Peer reviewed version

Link to published version (if available):
10.1063/1.4997790

Link to publication record in Explore Bristol Research
PDF-document

University of Bristol - Explore Bristol Research
General rights

Why morphology matters in birds and UAV's: How scale affects attitude wind sensitivity

L. L. Gamble, and D. J. Inman

Aerospace Engineering Department, University of Michigan, Ann Arbor, Michigan 48109, USA

Abstract

Though natural fliers have been shown to morph their geometry to adapt to unfavorable wind loading, there exists heavy skepticism within the aviation community regarding the benefits and necessity of morphing aircraft technology. Here we develop a vector derivation that characterizes how high winds affect the overall flight velocity and sideslip for both natural and manmade fliers. This derivation is formulated in such a way that only a single non-dimensional velocity parameter is needed to quantify the response. We show mathematically that in high winds, low-altitude fliers are more prone to substantial changes in sideslip angle, struggle to maintain gliding velocity, and experience five times the peak sideslip sensitivity when compared to high-altitude fliers. In order to counteract these adverse changes, low-altitude fliers require a high degree of controllability which can be achieved through extreme morphological changes. The results presented here highlight the importance of integrating morphing concepts into future low-altitude aircraft designs and provide a formulation to help designers decide whether or not to pursue adaptive morphing technology based on a single readily determinable parameter.

Birds, bats, and insects fly within the lower portion of the atmospheric boundary layer (ABL) at low speeds and are capable of extreme maneuverability through morphing wing camber, sweep, dihedral, etc. coupled with intricate tail movements [1-7]. Yet while the first entrepreneurs of aviation like Otto Lilienthal, John Montgomery and the Wright Brothers aspired to achieve bird-like flight stability and control through camber and wing warping [8-11], the quest for larger and faster air transportation produced heavy rigid aircraft with discrete control surfaces [12,13]. This allowed planes to carry heavier loads and fly at high speeds in the upper troposphere where the air is smooth. The troposphere exhibits semi-unidirectional currents due to the formation of Hadley cells, with most wind currents within 22° of the prevailing wind direction [14]. In contrast, low-altitude environments like the ABL are prone to unbiased winds due to local weather interactions and urban flow patterns [15], and are characterized by high turbulence levels approaching 50% in cities or urban environments with a wide range of turbulence length scales [16-18]. The following work derives a mathematical expression and subsequent analysis which explains analytically why natural fliers exhibit notable shape change during gliding flight, why the design of aircraft has shown minor development over the past 100 years, and which justifies the inclusion of morphing mechanisms in future designs of small unmanned aerial vehicles.

Historically, dating back to the 1930's, large-scale adaptive aircraft technologies have been forsaken at the price of heavy, multifaceted, and expensive designs [19]. The few concepts which have eclipsed these pitfalls, like the F-111 Aardvark and B-1 Lancer, are distinguish by their necessity to undergo large changes in wing loading [12] such as transitioning between loitering and high speed flight like birds of prey [3]. This focus on commanded changes in mission requirements overlooks the potential need to adapt to environmental disturbances in real time. In contrast, recent advances in morphing unmanned aerial vehicles (UAVs) [20-22] have targeted local shape change using smart materials like shape memory alloys and piezoelectrics, and have been motivated by sense-and-adapt (i.e. fly-by-feel) control methods [23,24] but have struggled to gain traction as a result of skepticism regarding their necessity and aerodynamic gain. The question

for engineers lingers, when is including adaptive morphing technology beneficial to aircraft design?

A straightforward vector derivation and sensitivity calculations were developed to demonstrate the effects of an in-plane wind on flyer attitude relative to the global coordinate system, aiming to both inform current research demonstrating the aerodynamic benefits of morphing geometry in birds, and justify the inclusion of morphing technology in small-scale low-altitude UAVs. This analysis describes the deviation in sideslip from gliding orientation in the absence of corrective measures such as wing morphing or actuator response. Gliding flight in particular represents a scenario in which a bird's wing geometry is not impacted by wing beat, providing a comparable scenario between aircraft and birds.

In gliding flight, the aircraft or bird experiences a forward velocity due to the thrust of the engine or intermittent wing flapping. This velocity can be represented as a vector ($\overrightarrow{U_\infty}$), describing both the magnitude and direction of flight, shown in Figure 1. However, in the event of wind incoming at an arbitrary angle (β_0), a second vector ($\overrightarrow{U_0}$) is introduced which will impact the resultant magnitude and direction of the flow that is observed by the body. Adding these separate velocity vectors forms a resultant vector ($\overrightarrow{U_R}$) which is dependent upon the relative magnitude and direction between the gliding velocity and wind velocity vectors. The angle (β) represents the sideslip angle or the angle of the resultant velocity vector relative to the gliding velocity. This implies substantially different responses between birds and aircraft which fly in very different flight conditions due to gliding velocity, altitude, and wind magnitude.
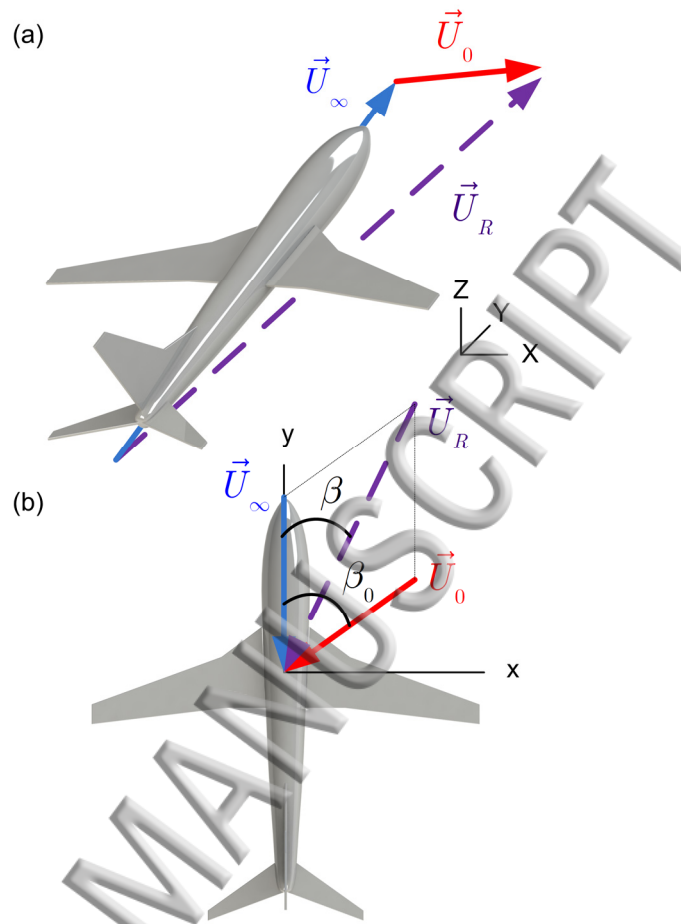
(a)

(b)

FIG. 1. Velocity vectors relative to a stationary body (a) Vector diagram in 3D relative to the global axis (X,Y,Z). (b) Vector diagram in 2D relative to the local body axis (x,y,z) considering only in-plane velocities.

Anticipating that the sideslip response will differ based on the ratio of the wind speed to the flight speed, characterizing these quantities across a spectrum of fliers is crucial. Figure 2 provides a visual comparison between a variety of fliers and their altitudes and turbulence environments. Table 1 shows that unlike aircraft, many natural fliers experience wind speeds equal to or greater than their range of flight velocities. The maximum non-dimensional wind speed ($\overline{U}_{max}$), calculated as the ratio of the maximum wind speed to the minimum glide speed, decreases for high-altitude fliers due to the large cruise speeds and relative lack of substantial winds in the upper troposphere. Low-altitude fliers such as natural fliers and UAVs experience a smaller maximum wind speed, but the corresponding wind magnitude is frequently larger than the flight speed. Though experimental data with both glide speed and corresponding wind speed is not widely available, the cruise speeds for a wide array of natural fliers has been well studied, showing glide speeds topping off at approximately 20m/s for heavier birds[25,26]. Thus the data presented in Table 1 roughly captures the full spectrum of natural fliers.
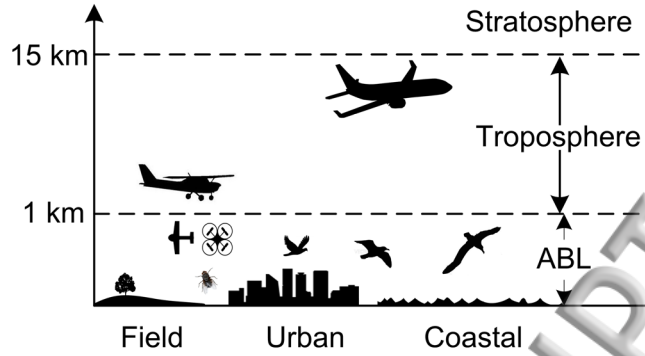
FIG 2. Visual representation of natural and engineered flier operational region and altitude

TABLE I. Comparison of non-dimensional wind speeds across a spectrum of fliers

	Flight Speed (m/s)		Wind Speed (m/s)			
Flyer	Min	Max	Min	Max	Measurement Environment	$\overline{U}_{max}$
Fly[25][i]	2	5	--	--	Field-Urban	4
Swallow[27]	3.7	19.4	1	6	Field	1.6
Gulls[15]	8.1	19.9	1.9	12.4	Urban-Coastal	1.5
Albatros[28]	9.1	17.9	5.6	12.5	Coastal	0.88
Fixed Wing UAV[29]	5.5	13.8	1.5	9.5	Field	1.7
	Cruise Speed (m/s)			Operating Altitude (km)		
Cessna Caravan[I]	100			7.6		.4
Pilatus PC-12NG[I]	144			9		.28
Boeing 777[I]	288			12		.14
	Wind Speed (m/s)					
Atmosphere	Min		Max		Measurement Altitude (km)	
Lower Troposphere[30]	2.5		8		--	
Upper Troposphere[31]	13		40		12	

i. Experimental data of the flight and corresponding wind speeds are reported where available. If no wind speed is available, the non-dimensional velocity is calculated using the appropriate atmospheric data provided. Data on aircraft flight speed and altitude is publically available.

Upon establishing the difference in $\overline{U}_{max}$ between low and high-altitude fliers, we derive the vector equations that govern the flight response as graphically described by Fig. 1b. Due to the definition of the problem statement, the gliding velocity vector consists of a single component in the negative y direction. The wind velocity vector may impact the body at an angle β_0, thus it contains components in both the x and y directions. Written in indicial notation, the x and y components (i and j respectively) are expressed separately. The expressions for the glide and wind velocity vectors are written as

$$\overrightarrow{U_\infty} = 0\text{i} - U_\infty\text{j} \tag{1}$$

and

$$\overrightarrow{U_0} = -U_0\sin(\beta_0)\text{i} - U_0\cos(\beta_0)\text{j} \tag{2}$$

4

where U_0 represents the magnitude of the wind vector, and U_∞ represents the magnitude of the glide vector. The resultant velocity vector is composed of both the wind velocity vector and the gliding velocity vector. Accordingly, using the principle of superposition, the two vectors can be added to obtain the resultant velocity vector by summing the respective i and j components

$$\overrightarrow{U_R} = \left(\overrightarrow{U_{\infty_i}} + \overrightarrow{U_{0_i}}\right) + \left(\overrightarrow{U_{\infty_j}} + \overrightarrow{U_{0_j}}\right) \tag{3}$$

where $\overrightarrow{U_{\infty_i}} = 0$, $\overrightarrow{U_{0_i}} = -U_0\sin(\beta_0)$, $\overrightarrow{U_{\infty_j}} = -U_\infty$, and $\overrightarrow{U_{0_j}} = -U_0\cos(\beta_0)$. For ease of analysis, the non-dimensional wind speed representing the ratio of wind disturbance to free stream magnitude is defined as $\bar{U} = \frac{U_0}{U_\infty}$ and the resultant velocity vector can be rewritten accordingly

$$\overrightarrow{U_R} = -\bar{U}U_\infty \sin(\beta_0)\,i - (U_\infty + \bar{U}U_\infty \cos(\beta_0))j \tag{4}$$

The vector $\overrightarrow{U_R}$ has both magnitude and direction. The magnitude of the non-dimensional resultant velocity vector can be calculated by taking the Euclidean Norm $\sqrt{\overrightarrow{U_{R_i}}^2 + \overrightarrow{U_{R_j}}^2}$, thus the resultant speed is described as

$$\bar{U}_R = \sqrt{(\bar{U}\sin(\beta_0))^2 + (1 + \bar{U}\cos(\beta_0))^2} \tag{5}$$

As was done previously, this quantity has been non-dimensionalized such that $\bar{U}_R = \frac{U_R}{U_\infty}$. Lastly, the direction of the vector, i.e. the equation for the resultant wind angle β, is then calculated using Pythagorean theorem: $\tan^{-1}\left(\frac{U_{R,i}}{U_{R,j}}\right)$, accordingly the sideslip angle is described by

$$\beta = \tan^{-1}\left(\frac{\bar{U}\sin(\beta_0)}{1 + \bar{U}\cos(\beta_0)}\right) \tag{6}$$

The system has overall been simplified from 3 unknowns (U_0, U_∞, and β_0), to 2 unknowns ($\bar{U}$, β_0) and allows the equations to be easily plotted and subsequently analyzed. Note that $|\beta_0| < 90°$ represents a tailwind (i.e. the y-components of the flight velocity and wind velocity are in the same direction) and $|\beta_0| > 90°$ represents a headwind, as this analysis has been performed relative to the local body axis (see Fig. 1). From this expression, we see mathematically how the sideslip angle and resultant speed are dependent upon the direction of the wind angle (β_0) and non-dimensional wind speed ($\bar{U}$). By definition, $\bar{U}$ must always be positive indicating that any changes in sign are the result of the β_0 contribution. This motivates segmenting the analysis into increments of 90° for which the sign of the sine and cosine terms alternate.

Our analysis shows that in tailwinds (Fig. 3a, d), the magnitude of the resultant sideslip angle increases with both $\bar{U}$ and β_0. For a given $\bar{U}$, increasing β_0 increases sideslip due to the addition of a velocity component perpendicular to the flight direction. Alternately, at a given β_0 the resultant sideslip is characterized by a rapid increase before plateauing and reaching steady-state. This steady-state, which only occurs at large non-dimensional speeds, was observed to equal the initial wind angle. These results imply that the attitude of low-altitude fliers is more heavily impacted than high-altitude fliers since they operate at greater $\bar{U}$ values and are more prone to experience larger incoming wind angles. In fact, the sideslip experienced by low-altitude fliers in tailwinds is up to 3 times larger than for high-altitude fliers.

In response to these changes in sideslip the flier may either restore the initial attitude such that the flier experiences no sideslip, or restore the initial flight course. With a high susceptibility to very large sideslip angles, low-altitude flyers require more drastic changes in control surface geometry, including greater rudder actuation and more efficient cambered actuation, to achieve either of these responses.

For headwinds (Fig. 3b, c), the response is much more complex and depends upon whether or not the wind speed is greater or less than the gliding speed. When $\bar{U}$ is greater than 1, the sideslip exhibits a similar response to tailwinds, though the sideslip angle is almost twice as large. Furthermore, low-altitude fliers may experience a resultant sideslip greater than 90°, representing a scenario where the resultant velocity vector no longer has a forward component. This phenomenon only occurs in the region of low-altitude fliers and is most severe in direct tailwinds, where the sideslip may reverse entirely from 0° to 180°. The flier would require greater propulsion (thus decreasing $\bar{U}$) to return to forward flight. When $\bar{U}$ is less than 1, the sideslip of high-altitude fliers does not always increase with β_0 and is most succinctly described by the rightward shifting point of inflection with increasing wind angle. The sideslip is hardly affected as the wind approaches a direct headwind and the overall sideslip angle is up to an order of magnitude smaller than that of low-altitude fliers.

Though not evident from Fig. 3, another detriment of headwinds is their tendency to asymmetrically affect the wing loadings in swept wing configurations. An angled headwind will impact the forward wing's leading edge, increasing its lift. This asymmetric lift induces roll which can lead to instabilities, tip stall and loss of actuator authority. One method of preventing this would be to decamber the wing to decrease lift and locally adjust the twist to decrease the angle of attack at the tips and prevent stall. Since the sideslip response is symmetric about the gliding direction (Fig. 3c, d), further analysis will focus solely on sideslip angles between 0° and 180°.
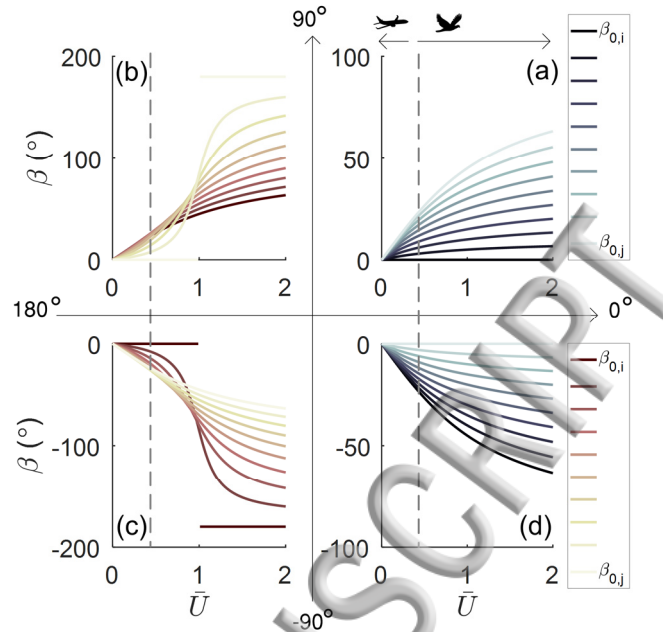
FIG 3. Sideslip response with respect to incoming wind magnitude and direction. Data is grouped by quadrants, read counterclockwise starting from quadrant 1. Legend is written in indicial notation of the form $\beta_{0,i} - \beta_{0,j}$ for conciseness. For example in quadrant a, $\beta_{0,i}$ and $\beta_{0,j}$ corresponds to $\beta_{0,0}$ and $\beta_{0,90}$ respectively. The dashed line marks the divide between low and high-altitude flyer $\bar{U}_{max}$.

Given these drastically different sideslip curves discussed prior, it is clear that sideslip may be more susceptible to changes in wind speed and angle under certain conditions. A sensitivity parameter is introduced, represented as $\frac{\partial \beta}{\partial \bar{U}}$, which describes the degree to which changes in $\bar{U}$ affect sideslip angle. It is important to note that here $\bar{U}$ is being used to analyze the dynamic affect of wind on sideslip angle by assuming a constant glide speed, and thus variations in $\bar{U}$ are the result of changes in wind speed with time.

High-altitude fliers are most sensitive in tailwinds, and the sensitivity intensifies with increasing wind angle (Fig. 4a). However, even though variations in wind speed caused by turbulent environments are prone to causing variations in sideslip for high altitude fliers, the resultant sideslip is quite small as seen in Fig. 3, therefore; any resulting oscillations would be small amplitude. As the sideslip plateaus, the sensitivity decreases substantially. This trend is partly extended for winds above 90° (Fig. 4b); however, the trend shows a strong peak in sensitivity as $\bar{U}$ approaches. Physically, these peaks are the result of the headwind magnitude and direction being so large that the resultant velocity vector reverses in direction in a snap-through-like phenomenon. Low-altitude fliers in particular are extremely sensitive as winds approach direct headwinds with over 5 times the maximum sensitivity for tailwinds (Fig. 4c). These peaks in sensitivity correspond to the points of inflection in the sideslip curves shown in Fig. 3 and further indicate that low-altitude fliers are subject to these large increases in sensitivity for a broader range of wind angles (Fig. 4d), as high altitude fliers do not experience adequate wind magnitudes to induce this phenomenon. This represents a dangerous scenario for low-altitude fliers where the magnitude of the sideslip angle and the sensitivity are both very large and is of

particular concern in low-altitude highly turbulent environments where the wind velocity may fluctuate rapidly with time resulting in high amplitude oscillations if left uncorrected. High frequency actuator mechanisms which are capable of undergoing large scale deformation would be needed to negate these effects.
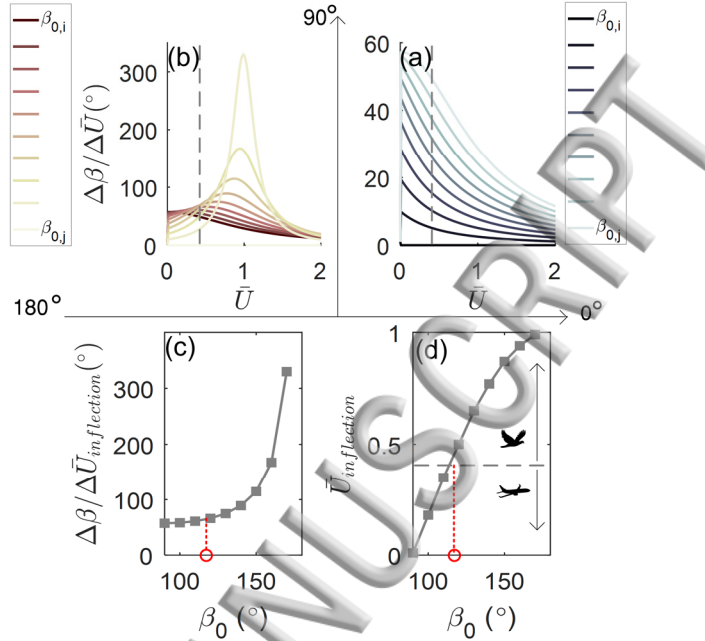

FIG 4. Effects of wind on sideslip sensitivity (a) Tailwind sensitivity (b) Headwind sensitivity (c) Peak sensitivity at points of inflection. (d) Non-dimensional speed at points of inflection. The red markers indicate the separation between peak sensitivity in low and high-altitude fliers with respect to wind angle, further highlighting that low-altitude fliers are subject to much larger peak sensitivity across a wider range of wind angles.

While winds influence the direction of flight by altering the sideslip angle, they also affect the resultant wind speed by effectively altering the flight speed relative to the ground. In tailwinds (Fig. 5a), $\overline{U}_R$ is always greater than 1, signifying that the resultant speed is greater than the original glide speed for both low and high-altitude fliers, since the wind vector and gliding vector both have negative j components. However, low-altitude fliers exhibit much larger $\overline{U}_R$ values particularly in direct tailwinds. For headwinds (Fig. 5b), the response decreases due to the addition of a j component in the opposite direction. As is indicated by values of $\overline{U}_R$ less than 1, both low and high-altitude fliers can experience a decrease in resultant speed from the gliding speed. However for large values of $\overline{U}$, the sideslip angle may also exceed 90° (shaded in gray), meaning that the flier would no longer have a forward velocity. This phenomenon only occurs in low-altitude fliers. Overall, low-altitude fliers experience a much larger range in $\overline{U}_R$, and thus are not able to maintain their initial glide speed as effectively as high-altitude fliers.

Though seemingly harmless, the consequences that arise due to the inability to properly regulate flight speed are further exacerbated by the fact that the flier's lift force is proportional to the squared speed:

$$L = \frac{1}{2}\rho A C_l U_R^2$$

(8)

8

where L is the force of lift, ρ is the air density, A is the lifting surface area, and C_l is the lift coefficient. In steady level flight, the force of lift equals the weight of the flier and thus the flier is neither loosing or gaining altitude[32]. But if for example a low-altitude flier's speed was halved as the result of heavy winds ($\bar{U}_R = 0.5$), then the corresponding lift force would effectively be a quarter of the original value and the flier would have a significant downwards acceleration. The flier would need to adapt its geometry to return to its original lift state. This is most effectively achieved by either changing the wing span by extending or folding the wings, or changing the total wing camber.
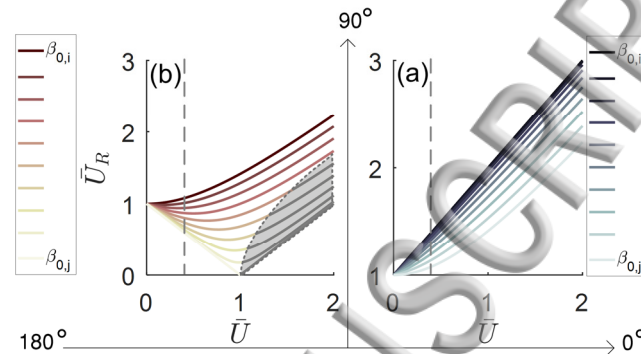

FIG 5. Maintaining glide speed is a challenge for low-altitude fliers (a) Headwind non-dimensional glide magnitude (b) Tailwind non-dimensional glide magnitude

Altitude, and ultimately scale, greatly influences the degree to which wind disturbances affect gliding flight in both natural and manmade fliers. Exposed to higher sideslips, peak sensitivity, and resultant speeds, low-altitude fliers like insects, birds and small UAVs must counteract these disturbances rapidly through large changes in geometry in order to maintain their initial heading and proper control of attitude and glide speed as is seen in nature[3,5]. The demand for both high speed and large scale deformations begs for the implementation of morphing actuators and mechanisms. For small UAVs, actuators like soft actuators, microrobotics and smart materials provide a unique solution that can accommodate large strains, rapid actuation and low profiles for small-scale integration[21,22]. While mid to high-altitude aircraft can still benefit from modern morphing technologies from an efficiency and mission-adaptive standpoint[12], this work reinforces the need to incorporate morphing technologies in future designs of low-altitude aircraft and UAVs to properly maintain control authority and effectiveness in unpredictable aerodynamics.
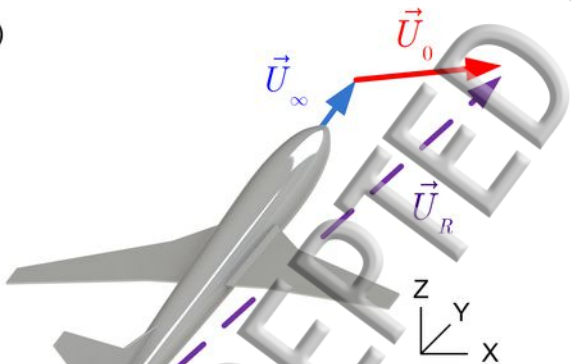
References
1. U. K. Müller and D. Lentink, Science **306,** 1899 (2004).
2. D. Lentink, U. K. Müller, E. J. Stamhuis, R. De Kat, W. Van Gestel, L. L. M. Veldhuis, P. Henningsson, A. Hedenström, J. J. Videler, and J. L. van Leeuwen, Nature **446,** 1082 (2007).
3. J. A. Gillies, A. L. R. Thomas, and G. K. Taylor, J. Avian Biol. **42,** 377 (2011).
4. V. A. Tucker, J. Exp. Biol. **133,** 33 (1987).

5. C. J. Pennycuick, J. Exp. Biol. **49,** 509 (1968).
6. R. Kumar and S. Shkarayev, Int. J. Micro Air Veh. **7,** 159 (2015).
7. A. P. Willmott and C. P. Ellington, J. Exp. Biol. **200,** 2705 (1997).
8. C. H. Gibbs-Smith, Nature. **198,** 824 (1963).
9. F. E. C. Culick, AIAA J. **41,** 985 (2003).
10. P. L. Jakab, Am. Hist. Rev. **98,** 1311 (1991).
11. G. D. Padfield and B. Lawrence, Ae. J. **109,** 421 (2005).
12. T. A. Weisshaar, J. Aircraft. **50,** 337 (2013).
13. R. G. Grant, Flight: 100 Years of Aviation. Duxford Kindersley, London, (2002).
14. A. Gettelman, D. E. Kinnison, T. J. Dunkerton, and G. P. Brasseur, J. Geophys. Res. D. **109,** D22101 (2004).
15. E. L. C. Shepard, C. Williamson, and S. P. Windsor, Phil. Trans. R. Soc. B. **371,** 20150394 (2016).
16. M. Roth, Q. J. R. Meteorol. Soc. **126,** 941 (2000).
17. J. R. Garratt, Earth-Sci. Rev. **37,** 89 (1994).
18. R. W. Macdonald, Bound.-Layer Meteor. **97,** 25 (2000).
19. S. Barbarino, O. Bilgen, R. M. Ajaj, M. I. Friswell, and D. J. Inman, J. Intell. Mater. Syst. **22,** 823 (2011).
20. L. L. Gamble, A. M. Pankonien, and D. J. Inman, AIAA **55,** 2956 (2017).
21. B. Sanders, F. E. Eastep, and E. Forster, J. Aircr. **40,** 94 (2003).
22. O. Bilgen, K. B. Kochersberger, and D. J. Inman, Aeronaut. J. **133,** 385 (2009).
23. N. Salowitz, Z. Q. Guo, Y. H. Li, K. Kim, G. Lanzara, and F. K. Chang, J. Compos. Mater. **47,** 97 (2012).
24. C. W. Ray, Smart Mater. Struct. **24,** 115026 (2015).
25. H. Tennekes, The MIT Press, Cambridge, (2009).
26. T. Alerstam, M. Rosén, J. Bäckman, P. G. Ericson, and O. Hellgren, PLoS Biol. **5,** 197 (2007).
27. D. R. Warrick, T. L. Hedrick, A. A. Biewener, K. E. Crandell, and B. W. Tobalske, Phil. Trans. R. Soc. B. **371,** 20150391 (2016).
28. L. B. Spear, and D. G. Ainley, Ibis **139,** 234 (1997).
29. S. Watkins, J. Milbank, B. J. Loxton, and W. H. Melbourne, AIAA J. **44,** 2591 (2006).
30. E. Kalnay, M. Kanamitsu, R. Kistler, W. Collins, D. Deaven, L. Gandin, M. Iredell, S. Saha, G. White, J. Woollen, *et al.,* Bull. Am. Meteorol. Soc. **73,** 437 (1996).
31. M. W. Burley, E. M. Ritchie, and C. R. Gray, Mon. Weather Rev. **85,** 11 (1957).
32. L. V. Schmidt, AIAA Education Series, Reston, Virginia, (1998).

(a)

$\vec{U}_0$

$\vec{U}_\infty$

$\vec{U}_R$

Z

Y

X

(b)

y

$\vec{U}_\infty$

β

$\vec{U}_R$

β_0

$\vec{U}_0$

x

	Stratosphere
15 km	
	Troposphere
1 km	
	ABL
Field	Urban	Coastal